Geomechanics and Engineering, *Vol. 38, No. 2 (2024) 179-189*
https://doi.org/10.12989/gae.2024.38.2.179

Design and optimization of layout patterns for rock TBM cutterheads

Ebrahim Farrokh*

Amirkabir University of Technology (Tehran Polytechnic), Hafez Ave., Tehran, Iran

(*Received August 16, 2023, Revised May 23, 2024, Accepted July 15, 2024*)

Abstract. This paper presents a geomechanical framework for designing and optimizing layout patterns of cutterheads for rock Tunnel Boring Machines (TBMs), aiming to enhance their engineering performance. By examining the forces and moments exerted by rock, the study addresses geometric constraints associated with cutter boxes in key regions of the cutterhead, including the center, face, and gage areas, as well as the three-dimensional effects of cutterhead curvature on the geometric constraints of the back of the cutter boxes in the gage area. Novel formulas are proposed for determining the center points of cutter boxes and calculating both the minimum angular spacing and distance spacing between consecutive cutter boxes along a spiral path. The paper outlines an optimized layout design process for four cutterhead configurations: random, random paired, radial, and double spiral designs. Examples are provided to illustrate the results of applying these designs. The findings underscore the efficacy of the proposed methods in achieving a uniform and symmetrical distribution of cutters and buckets on the cutterhead surface. This approach effectively eliminates boundary overlap and minimizes unbalanced forces and moments. From a geomechanical standpoint, this framework offers a robust strategy for enhancing the performance and reliability of TBM cutterheads in rock tunneling operations.

Keywords: bucket; cutter box; cutterhead; hard rock; layout design; optimization; overlap; TBM

1. Introduction

Optimizing the layout design of TBM cutterheads is essential for enhancing performance and increasing the durability of the main bearing. The arrangement of cutters, buckets, and manholes, known as the "Lace design" (Lislerud 1997), plays a critical role in preventing cutterhead deviation, vibration, and stress concentration during operation. Models based on cutting force estimation can be employed for both optimizing cutterhead design and estimating performance. Additionally, real-time acceleration data obtained through comprehensive testing can provide valuable insights into cutterhead behavior. The design of the cutterhead has a direct impact on cutting efficiency, balance, cutter life, and the maintenance of the main bearing and gearbox (Yang *et al*. 2023, Lin *et al*. 2019).

The layout design for rock TBM cutterheads encompasses both the cross-section profile and the surface profile of the cutterhead. The cross-section profile design primarily focuses on the arrangement of cutters on the head profile, especially in the curved area known as the gage region. Numerous studies have concentrated on optimizing the parameters related to the cross-section profile. Specifically, they have addressed the optimization of performance parameters (e.g., Han *et al*. 2019, Pan *et al*. 2019, Pan *et al*. 2018, Thyagarajan 2018, Han *et al*. 2017, Xia *et al*. 2015), the optimum cut geometry parameters such as penetration and spacing (e.g., Pourhashemi *et al*. 2022, Kim *et al*. 2020, Qi *et al*. 2016, Farrokh *et al*. 2015, Abu Bakar 2012, Cho *et al*. 2013, Hassanpour *et al*. 2009, Tuncdemir 2008, Zhao *et al*. 2007, Eskikaya *et al*. 2005, Gertsch *et al*. 2007, Lislerud 1997, Ozdemir *et al*. 1978, Rostami 2008, 1997, 1993, Roxborough *et al.* 1975), and the geometry and wear of cutting tools (Shao *et al.* 2023, Kim *et al.* 2022). Given that these aspects have been extensively covered using various methods in the literature, they will not be discussed in detail in this paper.

The cutterhead surface profile primarily addresses the geometric constraints of the structural elements of the cutterhead, including the cutter boxes, buckets, and pedestals. In optimizing the layout design for the cutterhead surface, it is crucial to minimize off-axis forces and moments and ensure that the position error of the centroid of the cutters does not exceed an allowable value (Huo *et al*. 2011a, b, 2010, Sun *et al*. 2018). In the industry, various layout designs are currently employed, including random, random paired, radial, and spiral designs (Farrokh 2021a, b, 2020, Rostami and Chang 2017, Huo *et al*. 2010, Rostami 2008). One important note about the conducted cutterhead layout designs is that, in the majority of them, the geometric constraints of the cutter boxes, buckets, and other crucial structural elements (e.g., cutterhead arms/pedestals) are not considered. If these geometric constraints are ignored, the tips of the cutters may be arranged so closely that the design pattern becomes impractical to implement. This issue is particularly significant in the center area, where space is limited, and in the gage area, where buckets must be incorporated into the design along with the cutter boxes. Additionally, the problem of overlapping control of the structural elements is inherently a 3D issue, especially in the back area of the gage region, where there is much less space compared to the front surface of the cutterhead.

*Corresponding author, Ph.D.
E-mail: e.farrokh@aut.ac.ir

ISSN: 2005-307X (Print), 2092-6219 (Online)

This study will focus exclusively on the cutterhead surface layout design. In this context, the geometric constraints of the cutter boxes are examined and formulated to prevent any overlap among the cutter boxes and other structural elements. To address the limited space behind the gage area of the cutterhead, the projection of the back of the cutter boxes is considered. The following sections of the paper will detail the developed formulas that describe these geometric constraints and their application to the four major layout designs mentioned above. To provide a clearer understanding of these formulas, their implementation and the final optimized results will be illustrated with examples. This paper specifically examines a geological scenario where the tunnel face consists of rock conditions, and the TBM cutterhead employs disc cutters as the main cutting tools. It is important to highlight that the study does not cover mixed face conditions, which involve the use of large cutterhead openings and various soft ground tools, including scrapers and/or rippers.

$$S_{opt} = 87.85 - 0.0239\,UCS - 1.663\,RT - 1.027 \quad (1)$$

$$(\frac{S}{p})_{opt} = 4.83 + 0.04\,UCS + 2.486\,RT \quad (2)$$

where S_{opt} is optimum cutter spacing in mm, $(\frac{S}{p})_{opt}$ is the optimum spacing over penetration ratio, UCS is the uniaxial compressive strength in MPa, and RT is the rock type code (1 for sedimentary rocks, 2 for volcanic rocks, 3 for metamorphic rocks, and 4 for granitic rocks).

Once the optimum spacing is identified, the arrangement of the disc cutters on the cutterhead is laid out, with adjustments made for the gage cutters to account for lateral forces and impacts. A lace design is then developed for the cutterhead surface, ensuring that each cutter follows a separate path. Symmetric configurations are preferred to balance forces and moments, although optimization is necessary to achieve a practical balance within the geometrical constraints. This involves adjusting the angular positions of the cutters while considering potential conflicts with cutter boxes, buckets, and cutterhead arms/pedestals. Additionally, the final design must consider the structural strength of the cutterhead to ensure it can withstand operational stresses and loads.

For the purpose of design comparison in the following sections, the layout design of a TBM with a 7.21 m diameter is developed according to the steps outlined in Farrokh (2021a). This cutterhead is designed to excavate a tunnel in granite with a maximum uniaxial compressive strength (UCS) of 150 MPa. It is equipped with single-edge cutters that have a diameter of 432 mm (17 inches) and a tip width of 19 mm. For a single-edge disc of this size, the typical bearing capacity is 255 kN.

To calculate the head balance, the cutting forces, including normal, rolling, and side forces (Fn_i, Fr_i, Fs_i), should be defined for all cutters in the center, face, and gage areas. For the cutters in the center and face areas, the CSM model (Rostami 1997) can be used (Eqs. (3) and (4)).

$$F_n = \frac{2.12}{1000} \cdot T^{\frac{5}{6}} \cdot R^{\frac{5}{6}} \cdot \phi^{\frac{2}{3}} \cdot S^{\frac{1}{3}} \cdot UCS^{\frac{2}{3}} \cdot BTS^{\frac{1}{3}} \quad (3)$$

$$F_r = F_n \cdot \tan\frac{\phi}{2} \quad \phi = \cos^{-1}\frac{R-p}{R} \quad (4)$$

where F_n is cutter normal force in kN, F_r is rolling force in kN, UCS is uniaxial compressive strength in MPa, BTS is Brazilian tensile strength in MPa, p is penetration in mm, S is cutter spacing in mm, T is tip width in mm, R is cutter radius in mm, and ϕ is the contact angle between cutter and rock in rad.

According to the Rostami model (Rostami 1997), with 80% of the bearing capacity for the normal force (approximately 200 kN), a maximum penetration of 3 mm can be achieved when the UCS is at its maximum value of 150 MPa, and the cutter spacing is 80 mm. Based on the experimental formulas provided by Farrokh (2021a), the number of cutters in different areas of the cutterhead, the bearing capacity, and the radius of the gage region are determined (a tilt angle of 70 degrees, 11 gage cutters, and a radius of 450 mm for the gage area).

The cutterhead surface profile (Fig. 1) is set up according to the procedure outlined in Farrokh (2021a). The head balance formulas are established according to Eqs. (5)-(14) and Fig. 2 to calculate the cutterhead axial force (thrust) (F_z), off-axis forces (F_x and F_y), torque (M_z), and off-axis moments (M_x and M_y). The layout design process includes 8 center cutters (one quad cutter and two twin cutters).

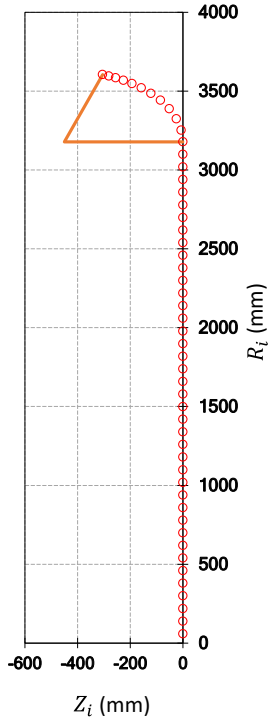

Fig. 1 The cross-section profile of a 7.21 m diameter cutterhead using single-edge cutters (Z_i represents the coordinate of the cutters along the depth of the cutterhead, R_i represents the radial position of the cutters on the cutterhead) (circles represent the tips of the cutters)

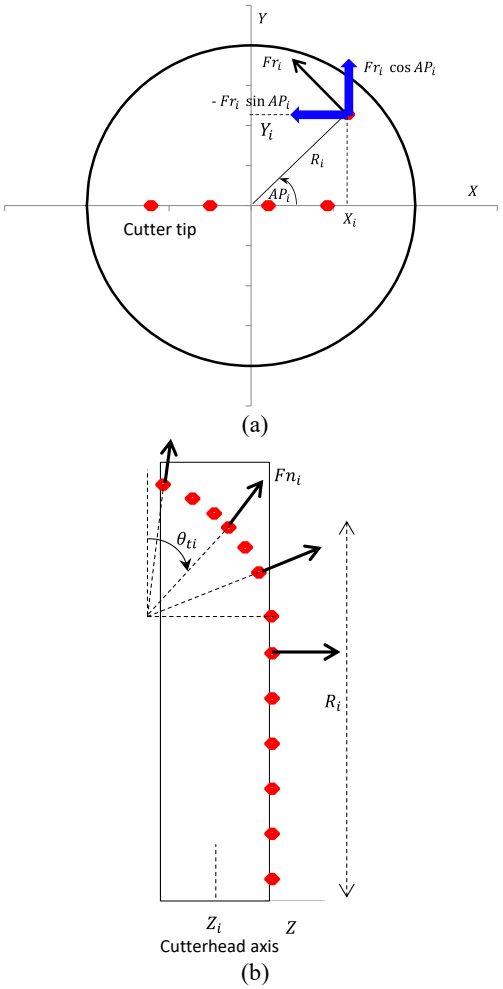

Fig. 2 (a) Rolling force applied to a cutter tip on the head profile and (b) Normal force applied to a cutter tip on the cross-section profile (dots represent the tips of the cutters) (Farrokh 2021a)

To study the pattern of the cutters on the cutterhead surface profile, the overlap of the cutter boxes must first be examined. This is to avoid placing the tips of the cutters too close together on the surface profile. A criterion is required to detect overlap between adjacent cutter boxes. Various patterns of cutter box allocation should then be formulated to achieve the final design. This procedure will be introduced in the next sections.

It should be noted that the current research focuses on rock conditions where only the cutter box, bucket, and cutterhead arms/pedestals are significant for the design. By considering rectangular boundaries for all these elements, the overlap control process among them remains consistent.

For illustration and comparison, the results of various patterns will be compared using the previously mentioned example.

$$X_i = R_i\, cos(AP_i) \tag{5}$$

$$Y_i = R_i\, sin(AP_i \tag{6}$$

$$X_c = \sum X_i \,/\mathrm{N} \tag{7}$$

$$Y_c = \sum Y_i \,/\mathrm{N} \tag{8}$$

$$F_x = \sum (Fn_i \cos(\theta_{ti})\ \cos(AP_i) - Fr_i \sin(AP_i)) \tag{9}$$

$$F_y = \sum (Fn_i \cos(\theta_{ti})\ \sin(AP_i) + Fr_i \cos(AP_i)) \tag{10}$$

$$F_z = \sum (Fn_i \sin(\theta_{ti})\ ) \tag{11}$$

$$M_x = \sum (Fy_i\, Z_i - Fz_i\, Y_i) \tag{12}$$

$$M_y = \sum (Fx_i\, Z_i - Fz_i\, X_i) \tag{13}$$

$$M_z = \sum (Fx_i\, Y_i - Fy_i\, X_i) \tag{14}$$

Fn_i : cutter normal force,
Fr_i : cutter rolling force,
Fs_i : cutter side force,
F_x, F_y , F_z : force components along the coordinate axes,
M_x, M_y, M_z : moments around the coordinate axes,
X_i , Y_i , Z_i : Coordinates of the cutters' tip position,
X_c , Y_c: Coordinates of the geometric centroid of the cutters' tip positions,
N: Number of cutters on the cutterhead,
θ_{ti} : Tilt angle of the cutters relative to the cutterhead surface,
R_i : Radial position of the cutter tip,
AP_i : The angular position of the cutters.

3. Study of cutter box overlap

To check the overlap of the cutter boxes, it is first necessary to calculate the coordinates of the four corner points around each box. In calculating these coordinates, two cases are considered:

Case 1: The center cutter, where the rectangle of the cutter box contains the center point of the cutterhead.

Case 2: Other boxes, where the center point of the cutterhead is not contained.

Fig. 3 and 4 illustrate the process of calculating these coordinates for the above cases.

The most important parameters shown in Fig. 3 and 4 are as follows:

P_1 to P_4 : The corner points of a cutter box
r_1 to r_4 : The radial positions of the corner points of a cutter box
AP_1 to AP_4 : The angle of the corner points of a cutter box
r_i : radial position of the tip of cutter number i
AP_i : The angle of the tip of the cutter number i
b_{wp} : The width of the cutter box in the direction of the cutterhead environment
b_{wr} : radial width of the cutter box

As shown in Fig. 5(a), in the gage region, cutter boxes are tilted with respect to the axis of the tunnel. This tilting

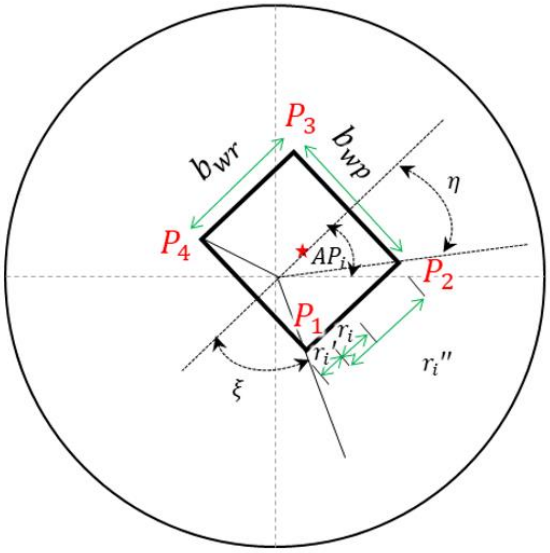

$$P_1\begin{pmatrix} r_1\cos AP_1 \\ r_1\sin AP_1 \end{pmatrix}$$
$$P_2\begin{pmatrix} r_2\cos AP_2 \\ r_2\sin AP_2 \end{pmatrix}$$
$$P_3\begin{pmatrix} r_3\cos AP_3 \\ r_3\sin AP_3 \end{pmatrix}$$
$$P_4\begin{pmatrix} r_4\cos AP_4 \\ r_4\sin AP_4 \end{pmatrix}$$

$$r_1 = r_4 = \sqrt{(r_i')^2+(\frac{b_{wp}}{2})^2}$$
$$r_2 = r_3 = \sqrt{(r_i'')^2+(\frac{b_{wp}}{2})^2}$$
$$r_i' = r_i - \frac{b_{wr}}{2}$$
$$r_i'' = r_i + \frac{b_{wr}}{2}$$
$$AP_1 = AP_i + 180 + \xi$$
$$AP_2 = AP_i - \eta$$
$$AP_3 = AP_i + \eta$$
$$AP_4 = AP_i + 180 - \xi$$
$$\xi = \text{atan}\frac{b_{wp}/2}{r_i'}$$
$$\eta = \text{atan}\frac{b_{wp}/2}{r_i''}$$

Fig. 3 The polar coordinates of the rectangle corner points of a cutter box containing the center point of the cutterhead (case 1)

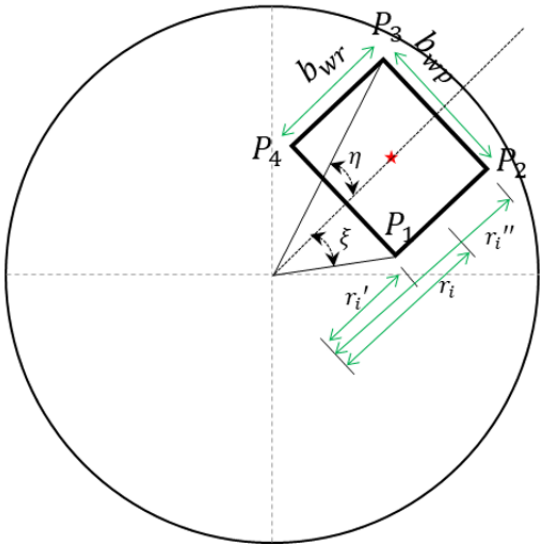

$$P_1\begin{pmatrix} r_1\cos AP_1 \\ r_1\sin AP_1 \end{pmatrix}$$
$$P_2\begin{pmatrix} r_2\cos AP_2 \\ r_2\sin AP_2 \end{pmatrix}$$
$$P_3\begin{pmatrix} r_3\cos AP_3 \\ r_3\sin AP_3 \end{pmatrix}$$
$$P_4\begin{pmatrix} r_4\cos AP_4 \\ r_4\sin AP_4 \end{pmatrix}$$

$$r_1 = r_4 = \sqrt{(r_i')^2+(\frac{b_{wp}}{2})^2}$$
$$r_2 = r_3 = \sqrt{(r_i'')^2+(\frac{b_{wp}}{2})^2}$$
$$r_i' = r_i - \frac{b_{wr}}{2}$$
$$r_i'' = r_i + \frac{b_{wr}}{2}$$
$$AP_1 = AP_i - \xi$$
$$AP_2 = AP_i - \eta$$
$$AP_3 = AP_i + \eta$$
$$AP_4 = AP_i + \xi$$
$$\xi = \text{atan}\frac{b_{wp}/2}{r_i'}$$
$$\eta = \text{atan}\frac{b_{wp}/2}{r_i''}$$

Fig. 4 The polar coordinates of the rectangle corner points of a cutter box that do not contain the center point of the cutterhead (case 2)

causes the back area of these cutter boxes to become closer to the tunnel axis, making their permissible allocation ring smaller (Fig. 5(b)). When a gage cutter box is viewed from the front, its radial width appears smaller than its actual radial width, while its peripheral width remains the same. To account for this 3D issue and simplify the calculation process in 2D, the back boundaries of the cutter boxes in the gage region can be projected onto the front face of the cutterhead. Once the coordinates of the back areas of the gage cutter boxes are identified, overlap control is then checked in 2D among the projected back area boundaries of the cutter boxes, instead of their front face boundaries.

The most important parameters shown in Fig. 5 are as follows:

b_{wr} : The actual radial width of the cutter box

$b_{wr(gage)}$: The projected radial width of the cutter box on the cutterhead surface

r_i : The radial position of the cutter tip i

d_p : The amount of protrusion of the tip of the cutter relative to the surface of the cutterhead

R_g : The radius of the curvature of the gage region

α_i : The tilt angle of the tip of the gage cutter with respect to the axis of the tunnel

Fig. 6 shows how to calculate the coordinates of the corner points for the buckets and pedestals.

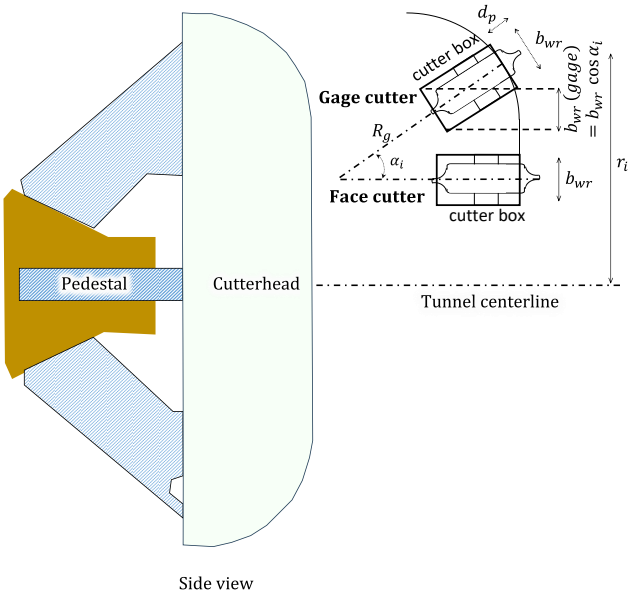

Side view

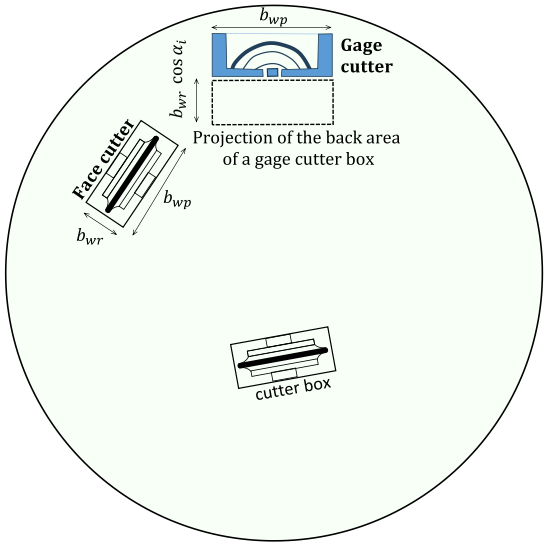

Front view

(a)

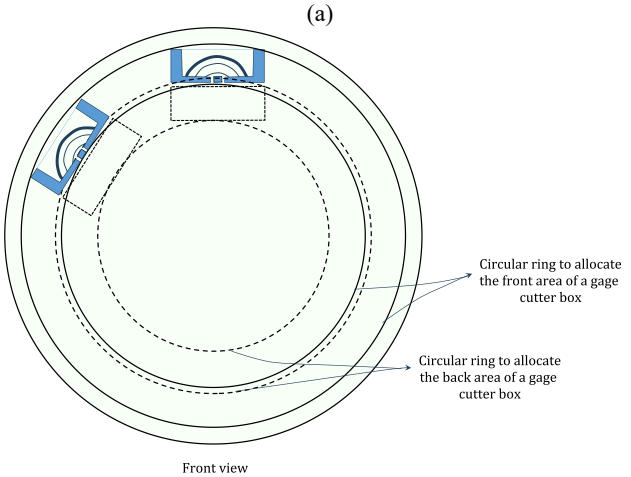

Front view

(b)

Fig. 5 (a) The projection of a gage cutter box back area on the cutterhead surface and (b) circular rings to allocate the front and back areas of a gage cutter box

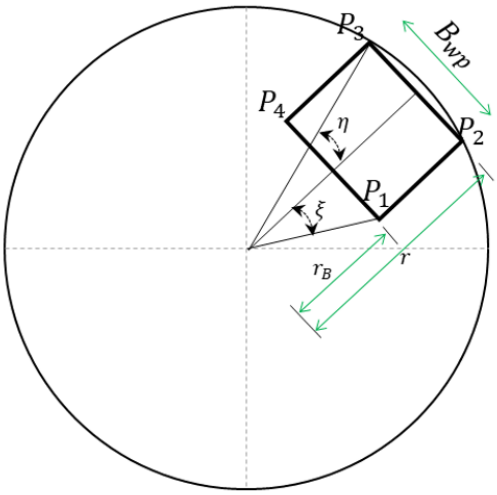

$$P_1\begin{pmatrix} r_1\cos AP_1 \\ r_1\sin AP_1 \end{pmatrix} \qquad r_1 = r_4 = \sqrt{(r_B)^2+(\frac{B_{wp}}{2})^2}$$

$$P_2\begin{pmatrix} r_2\cos AP_2 \\ r_2\sin AP_2 \end{pmatrix}$$

$$P_3\begin{pmatrix} r_3\cos AP_3 \\ r_3\sin AP_3 \end{pmatrix} \qquad r_2 = r_3 = \sqrt{(r)^2+(\frac{B_{wp}}{2})^2}$$

$$P_4\begin{pmatrix} r_4\cos AP_4 \\ r_4\sin AP_4 \end{pmatrix}$$

$$AP_1 = AP_i - \xi$$
$$AP_2 = AP_i - \eta$$
$$AP_3 = AP_i + \eta$$
$$AP_4 = AP_i + \xi$$
$$\xi = \operatorname{atan}\frac{B_{wp}/2}{r_B}$$
$$\eta = \operatorname{atan}\frac{B_{wp}/2}{r}$$

Fig. 6 The polar coordinates of the corner points of a bucket or pedestal

The most important parameters shown in Fig. 6 are as follows:

P_1 to P_4 : The corner points of a bucket or pedestal

r_1 to r_4 : The radial position of the corner points of a bucket or pedestal

AP_1 to AP_4 : The angular position of the corner points of a bucket or pedestal

r_B : The inner radial position of the corner points of a bucket or pedestal

r : radius of the cutterhead

B_{wp} : The peripheral width of the bucket or pedestal

Fig. 7 shows the criteria for determining the overlap between two adjacent cutter boxes using four sets of numbers calculated from the minimum and maximum x and y coordinates of the corner points of the corresponding cutter boxes. Overlap occurs when any corner point of the first rectangle falls within both the x and y ranges of the second rectangle. Similarly, if any corner point of the second rectangle falls within both the x and y ranges of the first rectangle, overlap occurs. If none of these conditions are met, no overlap occurs.

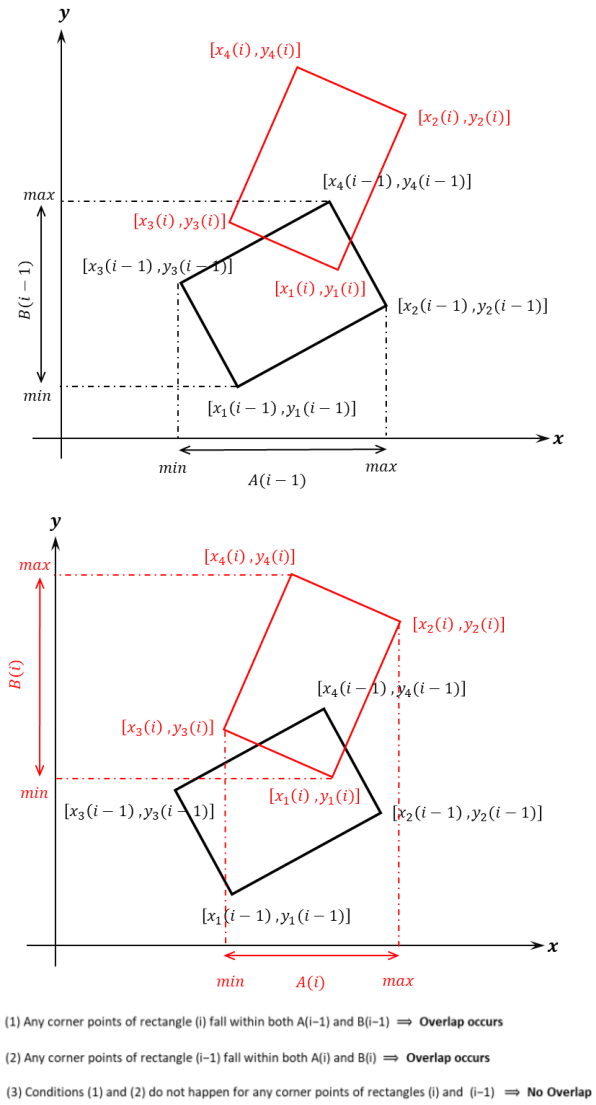

Fig. 7 Criteria to study the overlap of two adjacent cutter boxes

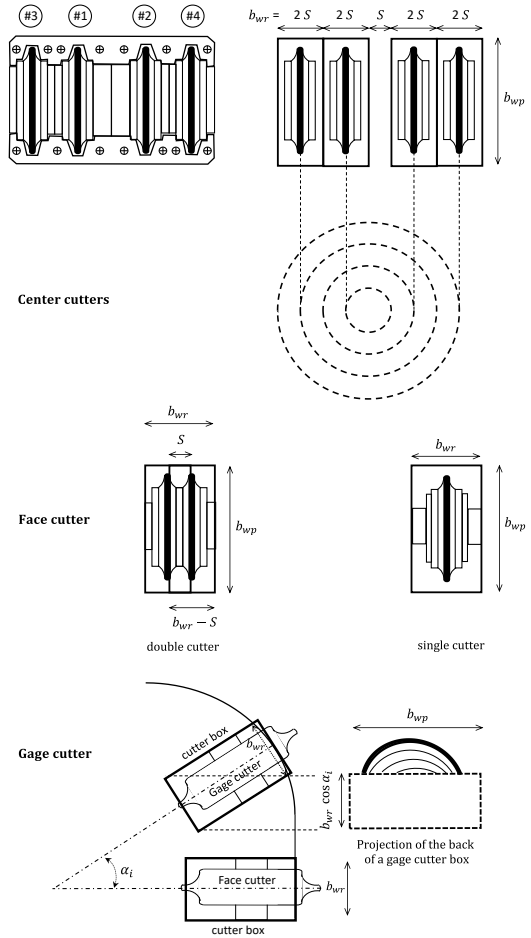

Fig. 8 Dimensions of various cutter boxes on the surface of the cutterhead

4. Allocating cutter boxes on the cutterhead surface

The random design method is used to ensure that no large empty areas are left on the cutterhead. To generate a design with balanced forces and moments, a random APi is generated, and the number of overlapping cutter boxes with each other, as well as with the buckets and pedestals, is checked. This process is repeated until a configuration with minimal overlap is achieved. This method is applied to each cutter box one by one. A drawback of this method is that allocating cutter boxes one by one with a random APi may not result in an optimal final pattern, as it may not have the lowest possible off-axis moments and forces. The random paired design can resolve this issue by assigning a paired cutter box with a complementary APi for each allocated cutter box.

The radial design is very simple; however, it has been reported to have a major drawback of leaving large free spaces on the cutterhead, especially in blocky ground (Burger and Dudouit 2009). The spiral design (commonly double spiral) aims to distribute the cutters more evenly on the surface, limiting the direct contact of large free blocks with the cutterhead surface (Farrokh 2021b). When large free blocks come into direct contact with the cutterhead surface, they rotate along with the cutterhead, leading to significant wear over time as the surface cannot break the blocks. To prevent this, the free rock blocks should be crushed by the tips of the cutters in front of the cutterhead surface, as the tips can apply concentrated forces to break the blocks into smaller pieces. Spiral designs are more effective in this regard.

According to studies by Geng *et al.* (2018), the double spiral design performs better in balancing torques and off-axis forces than radial and multiple spiral designs, thereby reducing cutter consumption. In massive hard rocks, double spiral and random (mostly random paired) designs have been successfully used in many projects.

The following sections briefly explain the formulas developed for some of these layout designs. The first step is to define the dimensions of the cutter boxes in the center, face, and gage areas. To simplify the overlap calculations, an individual cutter box boundary is considered for each cutter tip. For example, a quad-center cutter has four separate cutter box boundaries, and a double-disc has two

separate cutter box boundaries (Fig. 8). For gage cutters, the overlap of the back of the cutter boxes is more critical due to the limited space at the back of the cutterhead. Therefore, the projection of the back of the cutter boxes (Fig. 8) is considered in the overlap checking process.

4.1 Random design

The random design process begins by allocating buckets, pedestals (typically for micro TBMs), and the center cutter boxes (Fig. 9(a)). The position and length of the buckets are determined experimentally (Farrokh 2021b). For the center cutters, if a quad cutter is selected, the angular positions (AP) of the first four tips are set to (0°, 180°, 0°, 180°), corresponding to cutters no. (1, 2, 3, 4).

In the next step, all remaining cutter boxes are positioned on the horizontal axis with APi = 0° (Fig. 7(b)). The dimensions of the cutter boxes may vary for the face and gage cutters. For the gage cutters, the projection of the end of the cutter boxes on the cutterhead surface is used for the overlap check. A random APi is generated for the first face cutter, and its overlap with all previously allocated cutter boxes is checked. If any overlap is detected, a new APi is generated until the "no overlap" criterion is met (Fig. 9(b)). This process is repeated until all cutter boxes are allocated.

The resulting layout has no overlap; however, it is not the optimal layout design. To optimize the layout, the APis for all cutters in the face and gage regions are adjusted by a predetermined value (e.g., ±1°) one by one. If the overlap criterion is not violated, the configuration with the lowest off-axis forces and moments is selected. This process is repeated as needed until the lowest possible values for off-axis moments and forces are achieved.

Fig. 9(c) shows the final layout design achieved from this process for the cutterhead described in section 2 (with a 7.21 m diameter, 8 center cutters, 6 buckets, and a total of 51 cutters). Table 1 presents the results of the force and moment analysis for this design. The force and moment components are calculated as explained in section 2. The off-axis forces (F_x, F_y, F_s) and off-axis moments (M_x, M_y) have relatively small values, indicating good static balance (though not full balance). Additionally, the coordinates of the center of the cutters' positions (X_c, Y_c) are close to zero.

4.2 Random paired design

In this layout design, the angular position of a pair of cutters (two consecutive cutters with an angular spacing of 180 degrees) is assigned randomly. The first step is similar to the random design process, where the center cutters and buckets are allocated first. Next, all remaining cutter boxes are positioned on the horizontal axis with APi = 0°. A random APi is generated for the first face cutter, and its overlap with all previously allocated cutter boxes is checked. If any overlap is detected, a new APi is generated until the "no overlap" criterion is met (Fig. 7). The next cutter is a paired cutter, and its angular position is obtained by adding 180° to the previous cutter's angular position (Eq. (15)).

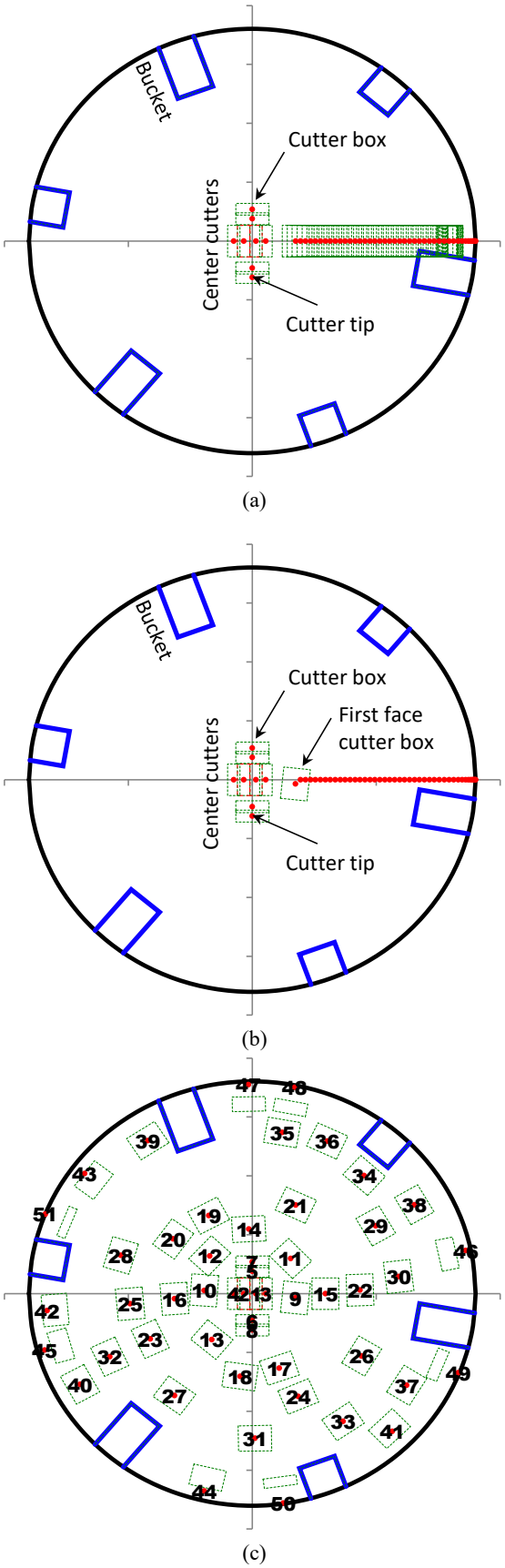

Fig. 9 An example of a random design for a 7.21 m diameter cutterhead: (a) initial pattern, (b) pattern with the first face cutter box allocated and (c) final optimized pattern

Table 1 The results of the static balance calculations for the random design shown in Fig. 9

Design type	F_x	F_y	F_z	F_s	M_x	M_y	M_z	X_c	Y_c
	kN	kN	kN	kN	kN-m	kN-m	kN-m	mm	mm
Random	-85	30	9038	91	0	91	1448	-11	20

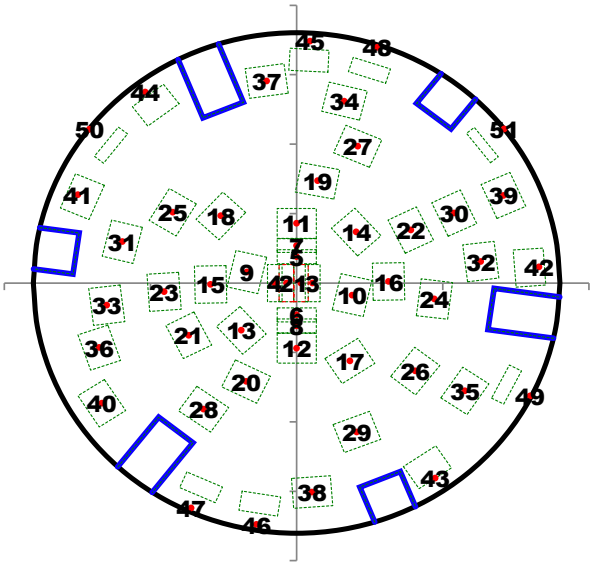

Fig. 10 An example of a random paired design for a 7.21 m diameter cutterhead

The results of the force and moment study for this design are similar to those shown in Table 1; therefore, they will not be repeated here.

4.3 Radial design

In the radial pattern, cutters are allocated along pre-specified radial lines on the cutterhead surface. This pattern is more commonly used in soft ground conditions, where the length of the buckets is typically longer compared to other patterns. This adjustment helps in handling the large volume of produced muck in front of the cutterhead more effectively.

In closed face shields, where the generated muck is transferred from the entire surface of the tunnel face, the buckets need to be extended towards the center. In such conditions, the radial pattern becomes the only viable solution.

The process of allocating the face and gage cutter boxes is similar to that explained for the random design, with the exception that the random APi is selected from a pre-specified list. In this list, the numbers have a special angular spacing, such as the set of (0°, 45°, 90°, 135°, 180°, 225°, 270°, 315°) as shown in the example in Fig. 11.

4.4 Double spiral design

The double spiral design benefits from both the paired design, where each cutter has a paired cutter, and an evenly distributed design, which ensures even angular or distance

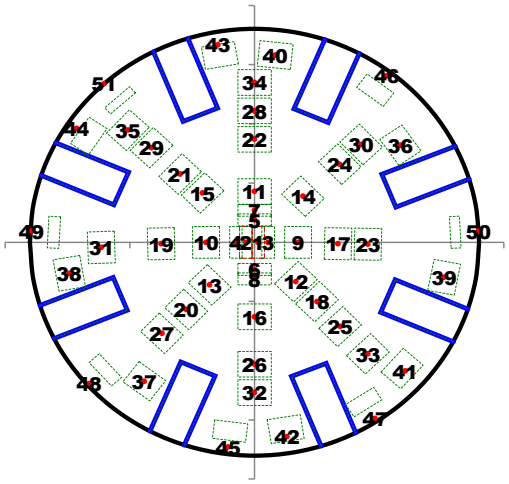

Fig. 11 An example of a 45° radial design for a 7.21 m diameter cutterhead

spacing between cutters. This combination results in the design having minimal large free spaces and low off-axis moments and forces even before the optimization process is conducted. As mentioned, each cutter has a paired cutter with a 180-degree angular spacing. To allocate a cutter on a spiral path, the minimum distance spacing between the centers of two consecutive cutter boxes (l) must be calculated first to avoid any overlap. To establish a criterion for calculating this distance, two parameters, l/d (distance over cutter box diameter) and b_{wp}/b_{wr} (peripheral box width over radial box width), are examined for various cases of cutter box dimensions. A relationship is then derived to determine the condition of "no overlap" using only the ratio of l/d (as shown in Fig. 12).

After determining the ratio of l/d, the minimum value of l (lmin) is calculated based on the dimension of the cutter box diameter (d). When allocating a new cutter box, assigning the angular position (AP) of the cutter tip becomes necessary. If the desired angular spacing (ΔAP) between the new cutter and the previously allocated cutter on the spiral path is achieved, the angular position of the new cutter can be easily calculated by adding the angular spacing to the angular position of the previously allocated cutter. Fig. 13 illustrates the process of calculating the angular spacing of a new cutter using the minimum distance spacing. Fig. 12(a) depicts the configuration of a double spiral pattern using the minimum angular spacing (ΔAPi as shown in Fig. 13). This initial pattern ensures that there is no overlap between consecutive cutter boxes in a spiral path; however, it leaves a large free space between the spiral paths. To reduce this free space and distribute the cutter boxes more evenly, the distance spacing (l) is increased, and the corresponding angular spacing is calculated according to Fig. 13.

To prevent overlap between the cutter boxes and the buckets, the distance spacing is adjusted near the buckets to push the boundaries of the cutter boxes outside the boundaries of the buckets. It's worth noting that the optimization process follows a similar approach to what was explained previously.

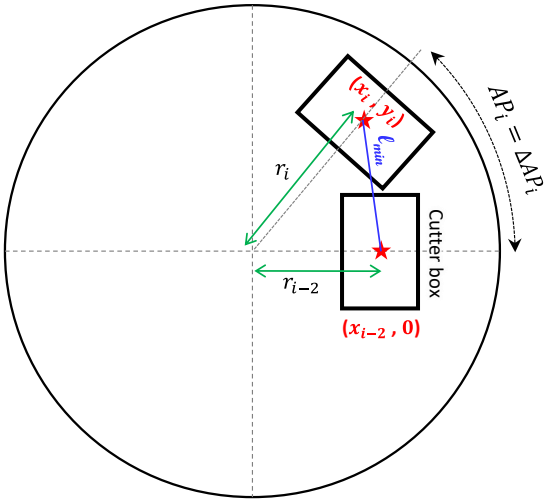

$$(x_i - x_{i-2})^2 + (y_i - 0)^2 = {l_{min}}^2$$

$$({x_i}^2 + {y_i}^2) + ({x_{i-2}}^2) - 2(x_i x_{i-2}) = {l_{min}}^2$$

$$x_{i-2}x_i = \frac{{r_i}^2 + {r_{i-2}}^2 - {l_{min}}^2}{2}$$

$$r_{i-2}\, r_i \cos \Delta AP_i = \frac{{r_i}^2 + {r_{i-2}}^2 - {l_{min}}^2}{2}$$

$$\Delta AP_i = \cos^{-1}\left|\frac{{r_i}^2 + {r_{i-2}}^2 - {l_{min}}^2}{2\, r_i\, r_{i-2}}\right|$$

Fig. 13 The minimum angular spacing between two consecutive cutter boxes as a function of minimum distance spacing between their central points

Fig. 14(b) provides an example of a spiral pattern using even distance spacing. In this example, the distance spacing is set to be 1.5 times the minimum required spacing.

Another approach in designing a double spiral pattern involves determining the minimum angular spacing between two consecutive cutter boxes in a spiral path without relying on the minimum distance spacing (as illustrated in Fig. 13). The angular position of the new cutter can then be easily calculated by adding the minimum angular spacing (angle θ_{min} as depicted in Fig. 15) to the angular position of the previously allocated cutter. Fig. 16(a) illustrates the configuration of a double spiral pattern using this minimum angular spacing approach. This initial pattern resembles the one shown in Fig. 14(a), with the key difference being that the formula to calculate θ_{min} is not dependent on the minimum distance spacing. To achieve a more even distribution of the cutter boxes, the minimum angular spacing is increased instead of the distance spacing (l). Fig. 16(b) showcases a double spiral pattern where the minimum angular spacing is added to the set of (2°,4°,6°,…). In this arrangement, the first face cutters (cutters number 9 and 10) are rotated further to ensure a larger distance spacing between the center cutters and these two cutters.

With this approach, a fixed angular spacing can also be implemented, provided that the selected value exceeds the minimum required angular spacing for all cutters.

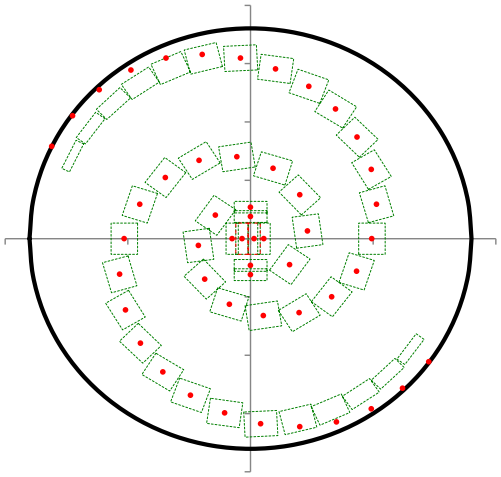

(a)

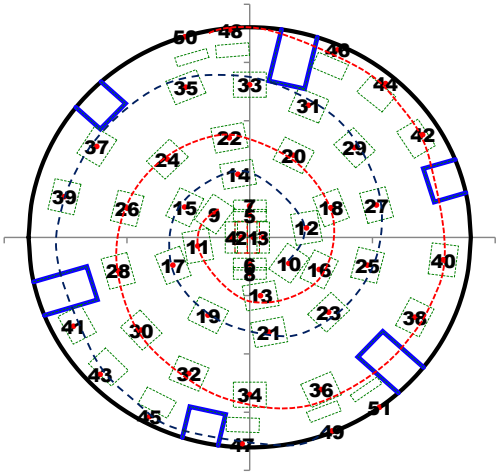

(b)

Fig. 14 Example of double spiral pattern generation using minimum angular spacing, and fixed distance spacing: (a) initial double spiral pattern with the use of minimum distance spacing and (b) final optimized pattern

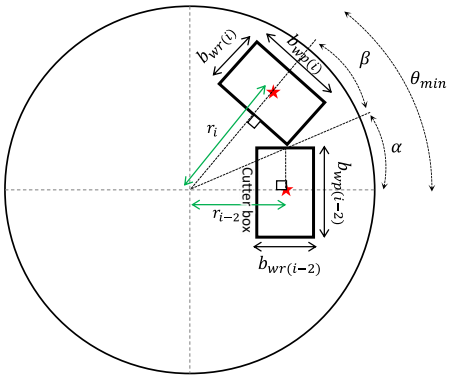

$$\theta_{min} = \alpha + \beta$$

$$\alpha = \tan^{-1}\left(\frac{\frac{b_{wp(i-2)}}{2}}{r_{i-2}}\right) \quad \beta = \tan^{-1}\left(\frac{\frac{b_{wp(i)}}{2}}{r_i - \frac{b_{wr(i)}}{2}}\right)$$

$$\alpha = \tan^{-1}\left(\frac{b_{wp(i-2)}}{2\, r_{i-2}}\right) \quad \beta = \tan^{-1}\left(\frac{b_{wp(i)}}{2\, r_i - b_{wr(i)}}\right)$$

Fig. 15 The minimum angular spacing between two consecutive cutter boxes as a function of dimensions of cutter boxes

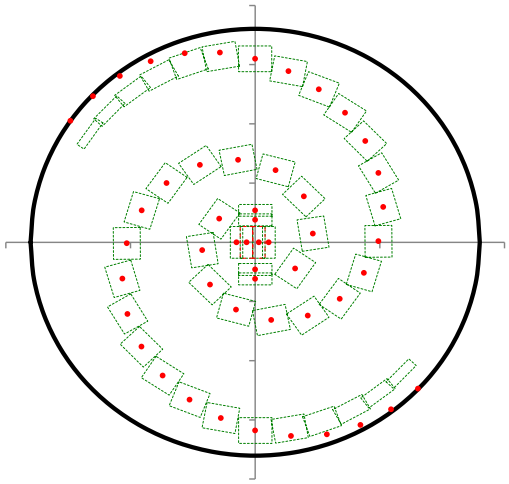

(a)

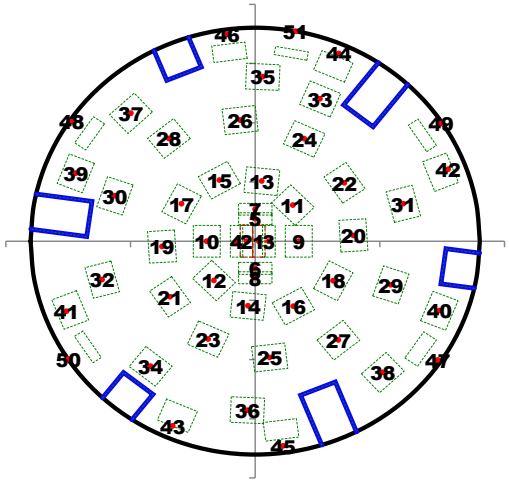

(b)

Fig. 16 Example of double spiral pattern generation using minimum angular spacing, and an increasing pattern of angular spacing: (a) initial double spiral pattern with the use of minimum angular spacing and (b) final optimized pattern

It is important to emphasize that the occurrence of overlaps between the cutter boxes and buckets is mitigated through the manual adjustment of the angular positions of the cutter boxes in proximity to the buckets.

By leveraging the aforementioned patterns, numerous layout designs can be formulated, enabling the design team to conduct a comparative analysis of their respective merits. This evaluation encompasses factors such as reduced off-axis forces and moments, as well as the simplification of bucket and pedestal designs. Subsequently, the most optimal design can be chosen through the application of engineering judgment.

5. Conclusions

This paper offers essential insights into the development of various cutterhead surface patterns, providing the necessary relationships for their design. The methods elucidated herein enable the detection of overlaps among structural elements, such as cutter boxes and buckets, and delineate the optimization process for these layouts.

The key findings of this study can be summarized as follows:

• The random design process can be automated through computer programs to verify all overlap constraints. However, the resulting design may not be optimized, necessitating a separate optimization procedure to minimize off-axis moments and forces.

•The paired random design is widely favored due to its capacity to reduce off-axis moments and forces, thus streamlining the optimization requirements.

• The double spiral pattern eliminates the need for randomization of angular positions, significantly reducing computation time. Nonetheless, manual inspection is necessary to adjust the angular positions of cutters near the buckets to ensure the absence of overlap.

• The radial layout closely resembles a random or random paired design, albeit with angular positions randomly assigned from a predetermined set of numbers. This pattern facilitates the extension of buckets further towards the center of the cutterhead.

The methodologies delineated in this paper offer pragmatic solutions for minimizing off-axis moments and forces, thereby enhancing performance and efficiency. By integrating geomechanical principles into the design process, this research contributes to the advancement of Tunnel Boring Machine (TBM) technology in rock tunneling applications, providing design engineers and practitioners with invaluable insights and tools.

References

Abu Bakar, M.Z. (2012), "Saturation effects on mechanical excavatability of sand rock under selected rock cutting tools", Ph.D. Dissertation, Missouri University of Science and Technology, USA.

Burger, W. and Dudouit, F. (2009), "The Hallandsås dual mode TBM", *Proceedings of the Rapid Excavation and Tunneling Conference*, Las Vegas, USA.

Cho, J.W., Jeon, S., Jeong, H.Y. and Chang, S.H. (2013), "Evaluation of cutting efficiency during TBM disc cutter excavation within a Korean granitic rock using linear-cutting-machine testing and photogrammetric measurement", *Tunn. Undergr. Sp. Tech.*, **35**, 37-54. https://doi.org/10.1016/j.tust.2012.08.006.

Eskikaya, S., Bilgin, N., Balci, C. and Tuncdemir, H. (2005), "From research to practice: Development of rapid excavation technologies", (Eds., Erdem & Solak), *Underground Space Use: Analysis of the Past and Lessons for the Future*. Taylor & Francis Group, London.

Farrokh, E. (2020), "Positioning the Peripheral Cutters in Hard Rock TBMs", *Tunn. Undergr. Sp. Tech.*, **9**(3), 207-228. https://doi.org/10.22044/tuse.2020.9509.1392.

Farrokh, E. (2021a), "Optimum design of the peripheral cutters' specification on the head profile for hard-rock TBMs", *Tunn. Undergr. Sp. Tech.*, **107**. https://doi.org/10.1016/j.tust.2020.103668.

Farrokh, E. (2021b), "Uniformly distributed lace design for hard

rock TBMs", *Tunn. Undergr. Sp. Tech.*, **110**. https://doi.org/10.1016/j.tust.2021.103829.

Farrokh, E., Kim, D.Y. and Kyung, S.B. (2015). "Rotary cutting test for hard-rock TBM pPerformance evaluation", *World Tunneling Conference*, Dubrovnik, Croatia.

Geng, Q., Bruland, A. and Macias, F.J. (2018). "Analysis on the relationship between layout and consumption of face cutters on hard rock Tunnel Boring Machines (TBMs)", *Rock Mech. Rock Eng.*, **51**, 279-297. https://doi.org/10.1007/s00603-017-1320-1.

Geng, Q., Wei, Z., Menga, H. and Maciasb, F.J. (2016), "Mechanical performance of TBM cutterhead in mixed rock ground conditions", *Tunn. Undergr. Sp. Tech.*, **57**, 76-84. https://doi.org/10.1016/j.tust.2016.02.012.

Han, D.Y., Cao, P., Liu, J. and Zhu, J.B. (2017), "An experimental study of dependence of optimum TBM cutter spacing on pre-set penetration depth in sandstone fragmentation", *Rock Mech. Rock Eng.*, **50**, 3209-3221. https://doi.org/10.1007/s00603-017-1275-2.

Han, M., Cai, Z. and Qu, C. (2019), "On the loads for strength design of cutterhead of full-face rock tunnel boring machine", *Chinese J. Mech. Eng.*, **32**. https://doi.org/10.1186/s10033-019-0411-1.

Hassanpour, J., Rostami, J., Khamehchiyan, M. and Bruland, A. (2009), "Developing new equations for TBM performance prediction in carbonate-argillaceous rocks: a case history of Nowsood water conveyance tunnel", *Geomech. Geoeng.*, **4**(4), 287-297. https://doi.org/10.1080/17486020903174303.

Huo, J., Sun, W., Chen, J., Su, P. and Deng, L. (2010). "Optimal disc cutters plane layout design of the full-face rock tunnel boring machine (TBM) based on a multi-objective genetic algorithm", *J. Mech. Sci. Tech.*, **24**(2), 521-528. https://doi.org/10.1007/s12206-009-1220-8.

Huo, J., Sun, W., Chen, J. and Zhang, Z. (2011a), "Disc cutters plane layout design of the full-face rock tunnel boring machine (TBM) based on different layout patterns", *Comput. Ind. Eng.*, **61**, 1209-1225. https://doi.org/10.1016/j.cie.2011.07.011.

Huo, J., Zhao, H., Zhang, X., Sun, W. and Zhao, Y. (2011b), "Cutters plane layout design of the full-face rock Tunnel Boring Machine (TBM) based on multi-spiral layout pattern", *Adv. Mater. Res.*, **308-310**, 1288-1291. https://doi.org/10.1016/j.cie.2011.07.011.

Kim, Y., Hong, J., Shin, J. and Kim, B. (2022), "Shield TBM disc cutter replacement and wear rate prediction using machine learning techniques", *Geomech. Eng.*, **29**(3), 249-258. https://doi.org/10.12989/gae.2022.29.3.249.

Kim, K.Y., Jo, S.A., Ryu, H.H. and Cho, G.C. (2020), "Prediction of TBM performance based on specific energy", *Geomech. Eng.*, **22**(6), 489-496. https://doi.org/10.12989/gae.2020.22.6.489.

Lin, L., Xia, Y., Li, Z., Wu, C., Cheng, Y. and Tan, Q. (2019), "Dynamic characteristics analysis with multi-directional coupling in a TBM mainframe", *Chin. J. Mech. Eng.*, **32**, 98. https://doi.org/10.1186/s10033-019-0412-0.

Lislerud, A. (1997), "Principles of mechanical excavation", Tamrock Corp, POSIVA 97-12.

Ozdemir, L., Miller, R. and Wang, F.D. (1978). "Mechanical tunnel boring prediction and machine design", NSF APR73-07776-A03. Colorado School of Mines. Golden, Colorado, USA.

Pan, Y.C., Liu, Q.S., Liu, J.P., Huang, X., Liu, Q. and Peng, X.X. (2018), "Comparison between experimental and semi-theoretical disc cutter cutting forces: Implications for frame stiffness of the linear cutting machine", *Arabian J. Geosci.*, **23**, 233-245. https://doi.org/10.1007/s00603-018-1400-x.

Pan, Y.C., Liu, Q.S., Peng, X.X., Liu, Q., Liu, J.P., Huang, X., Cui, X. and Cai, T. (2019), "Full-scale linear cutting tests to propose some empirical formulas for TBM disc cutter performance prediction", *Rock Mech. Rock Eng.*, **52**(5), 1803-1820. https://doi.org/10.1007/s00603-019-01865-x.

Qi, G., Zhengying, W. and Hao, M. (2016). "An experimental research on the rock cutting process of the gage cutters for rock tunnel boring machine (TBM)", *Tunn. Undergr. Sp. Tech.*, **52**, 182-191. https://doi.org/10.1016/j.tust.2015.12.008.

Pourhashemi, S.M., Ahangari, K., Hassanpour, J. and Eftekhari, S.M. (2022). "TBM performance analysis in very strong and massive rocks; case study: Kerman water conveyance tunnel project, Iran", *Geomech. Geoeng.*, **17**(4), 1110-1122. https://doi.org/10.1080/17486025.2021.1912410.

Rostami, J. and Chang, S.H. (2017), "A closer look at the design of cutterheads for hard rock tunnel-boring machines", *Engineering*, **3**(6), 892-904. https://doi.org/10.1016/j.eng.2017.12.009.

Rostami, J. (1993), "Design optimization, performance prediction and economic analysis of tunnel boring machine for the construction of the proposed Yucca Mountain nuclear waste repository", M.S. Thesis, Colorado School of Mines, Golden, Colorado, USA.

Rostami, J. (1997), "Development of a force estimation model for rock fragmentation with disc cutters through theoretical modeling and physical measurement of crushed zone pressure", Ph.D. Dissertation, Colorado School of Mines, Golden, Colorado, USA, p. 249.

Rostami, J. (2008), "Hard Rock TBM cutterhead modeling for design and performance", *Geomech. Tunn.*, **1**(1), 18-28. https://doi.org/10.1002/geot.200800002.

Roxborough, F.F. and Phillips, H.R. (1975), "Rock excavation by disc cutter", *Int. J. Rock Mech. Min. Sci. Geomech. Abstr.*, **12**(12), 361-366. https://doi.org/10.1016/0148-9062(75)90547-1.

Shao, X., Jiang, Y., Zhu, Z., Yang, Z., Wang, Z., Cheng, J. and Liu, Q. (2023), "TBM disc cutter ring type adaptability and rock-breaking efficiency: Numerical modeling and case study", *Geomech. Eng.*, **34**(1), 103-113. https://doi.org/10.12989/gae.2023.34.1.103.

Sun, H., Guo, W., Liu, J., Song, L. and Liu, X. (2018), "Layout design for disc cutters based on analysis of TBM cutter-head structure", *J. Cent. South Univ.*, **25**, 812-830. https://doi.org/10.1007/s11771-018-3786-8.

Thyagarajan, M.V. (2018), "The comparison of cutting forces on disc cutters in constant vs variable penetration modes", M.S. Thesis, Colorado School of Mines, Golden, Colorado, USA.

Tuncdemir, H., Bilgin, N., Copur, H. and Balci, C. (2008), "Control of rock cutting efficiency by muck size", *Int. J. Rock Mech. Min. Sci.*, **45**(2), 278-288. https://doi.org/10.1016/j.ijrmms.2007.04.010.

Xia, Y., Zhang, K. and Liu, J. (2015), "Design optimization of TBM disc cutters for different geological conditions", *World J. Eng. Tech.*, **3**(4). https://doi.org/10.4236/wjet.2015.34023.

Yang, Z., Wang, L., Zhou, J., Li, D., Zhang, K. and Guo, X. (2023), "Mechanical characteristics of a tunnel boring machine cutterhead during rock breaking: Physical model tests and transient dynamic analysis", *Adv. Mech. Eng.*, **15**(3). https://doi.org/10.1177/16878132231159971.

Zhao, Z., Gong, Q., Zhang, Y. and Zhao, J. (2007), "Prediction model of tunnel boring machine performance by ensemble neural networks", *Geomech. Geoeng.*, **2**(2), 123-128. https://doi.org/10.1080/17486020701377140.

JS